Preparation of ZrC/SiC composites by using polymer-derived ceramics and spark plasma sintering

Hatim Laadoua, William John Clegg, Nicolas Pradeilles, Romain Lucas, Sylvie Foucaud

Preparation of ZrC/SiC composites by using polymer-derived ceramics and spark plasma sintering

Hatim LAADOUA[1] ; Nicolas PRADEILLES[1] ; Romain LUCAS[1]*; Sylvie FOUCAUD[1] ; William John CLEGG[2]

[1] *Univ. Limoges, CNRS, IRCER, UMR 7315, F-87000, Limoges, France*

[2] *Gordon Laboratory, Department of Materials Science and Metallurgy,University of Cambridge, 27 Charles Babbage Rd, CB30FS, UK*

Corresponding author: Dr. R. Lucas, IRCER, UMR 7315
Centre Européen de la Céramique
12 Rue Atlantis, F-87068 Limoges Cedex, France
Tel: (+)33587502350

Fax: (+)33587502304

E-mail: romain.lucas@unilim.fr

Abstract: ZrC/SiC composites were fabricated using Spark Plasma Sintering (SPS) combined with the Polymer-Derived Ceramics (PDC) route. The originality of this work, consisted in the direct ceramization/sintering of a ZrC/polymer

mixture without any previous crosslinking steps. The presence of a polymer in our mixtures required an optimization of the thermomechanical parameters of SPS in order to promote the polymer-to-ceramic conversion prior to the densification. The optimized SPS conditions were composed of a dwell temperature of 700 °C for 10 minutes followed by a soaking temperature of 1700 °C for 5 min under an applied load of 75 MPa. A fine and homogenous phase distribution was achieved at relatively low temperature (1700 °C) compared to

the high temperatures required for the sintering of the refractory composite. The influence of the addition of SiC (up to 10wt%) was also studied and related to the final relative densities and mechanical properties of the composites.

Keywords: Manufacturing; Consolidation; Hybrid; Ceramic-matrix composites (CMCs)

1. Introduction

In application areas such as aeronautics, aerospace, or nuclear, the use of materials operating under extreme environmental conditions is required [1-3]. They include the family of carbides, which are non-oxide ceramics with a melting temperature higher than 2000 ° C and good mechanical properties [4]. Zirconium carbide is one of these carbides with a good refractoriness and interesting mechanical properties at high temperatures. However, it has a low oxidation resistance, which limits its use in the presence of oxygen at high temperature [5]. To overcome this problem, the use of composite materials based on silicon carbide is a promising route. Indeed, silicon carbide has, in addition to its thermomechanical properties close to those of ZrC, a passive oxidation resistance at high temperature, which limits the degradation of the material [6]. Thus, the combination of these two materials should generate high-performance ceramics.

For this, different approaches have been used to incorporate an SiC phase into the ZrC matrix in order to achieve well homogenous ZrC/SiC composites with the desired properties. Mixing and sintering of carbide powders is a commonly method to manufacture such composites. However, the densification of these carbides requires high sintering temperatures and pressure-assisted techniques to achieve dense bodies. For example, Zhao *et al.* [7] have reached relative densities of 86.6% for ZrC and 90.8% for ZrC/20vol% SiC by pressureless sintering at 1900 °C combined with high-energy ball milling. The increase of the sintering temperature to 2100°C has improved the relative densities of ZrC and ZrC/20vol% SiC to 98.4% and 96.7% respectively.

In this way, research has focused on the use of field-assisted sintering techniques such as Spark Plasma Sintering (SPS) to improve the densification without resorting to high sintering temperatures. Starting from ZrC and SiC powders, a fully dense (99% relative density) ZrC/SiC (10 vol%) composite can be obtained by SPS under vacuum at 1850 °C for 5 min and a uniaxial pressure of 40 MPa [8]. Despite the densification improvement of the composite by SPS, utilizing carbide powders as starting materials did not offer the possibility to control the shaping of materials as well as their chemical and microstructural homogeneity. Indeed, the latter may enhance the mechanical properties and the oxidation resistance of the composites.

In this aim, a promising route to manufacture ZrC/SiC composites known as the Polymer-derived Ceramics (PDC) is increasingly explored [9]. Indeed, the use of liquid preceramic polymers opens a new way to produce advanced multi-component ceramics by multiple techniques such as Precursor-Infiltration-and-Pyrolysis technique (PIP) [10,11] or by mixing a polycarbosilane as a source of SiC phase with carbide powder [12]. Nonetheless, the latter, requires a cross-linking step, which may induce an increase of the oxygen amount in the structure. In this work, well homogenous ZrC/SiC composites were prepared using an SPS technique and the PDC route.

A first part of the work consisted in controlling the quality of the synthesized ZrC powders in terms of chemical composition and particle size. The second part dealt with the mixing of these synthesized ZrC powders and a commercial preceramic polymer as SiC precursor. The peculiarity of our method lies in the ceramization/sintering of the prepared mixtures directly by SPS without prior

cross-linking. The optimization of sintering parameters was studied also and related to the final relative densities and microstructures of the composites.

2. Experimental procedure

2.1. Raw chemicals and powders

For the synthesis of ZrC powders, commercial zirconia (Alfa Aesar, Germany - purity 99.5%) and amorphous carbon black (Prolabo, France – purity 99.25%) were used as starting precursors. For the SiC phase, a commercially available preceramic polymer, the Allylhydridopolycarbosilane SMP10 (Starfire Systems Inc., USA) was utilized as received. It is a clear amber liquid with a theoretical molecular formula $[SiH\ (CH_2CH{=}CH_2)\ CH_2]_{0.1n}\ [SiH_2CH_2]_{0.9n}$ and a viscosity between 0.04 and 0.1 Pa.s at 25 °C.

2.2. Synthesis of ZrC powders and ball-milling process

The carbothermal reduction of zirconia has been employed to synthesize zirconium oxycarbide powders following the synthesis protocol presented in a previous paper [13]. Assuming a complete occupation of the octahedral sites of the fcc lattice of zirconium by carbon and oxygen, *i.e.* the sum of (C/Zr) and (O/Zr) is equal to 1; the carboreduction reaction can be expressed as follows:

$$ZrO_{2\,(s)} + (1+2x)\ C_{\,(s)} \Rightarrow ZrC_xO_{1-x\,(s)} + (1+x)\ CO_{\,(g)}$$

The carbon black and the commercial zirconia were mixed in mass proportions (77.96 wt% ZrO_2 and 22.04 wt% C) and then heat-treated at 1750 °C for 8 hours in a graphite resistance furnace (oven V.A.S., Suresnes, France) in an argon flow (30 $L.h^{-1}$) [13]. The obtained ZrC powders were agglomerated and therefore, required a ball-milling step to reduce their size and thus, improve the sinterability and the powder impregnation by the polymer.

Among the various ball-milling techniques, attrition milling of carbides seemed to give promising results [14]. For that, the synthesized powders were put in a container among with ZrO_2 beads (Netzsch, Germany, Ø = 0.8 mm) and 200 mL of distilled water. The ball to powder ratio (BPR) was fixed at 10:1 in weight. The suspension was then stirred at 2000 rpm for one hour to obtain strong shearing forces and then dried in an oven (110 ° C). Once the desired granulometry is achieved, the powders were mixed with the commercial polymer in order to prepare the ZrC/polymer systems.

2.3. Preparation of the mixture (ZrC/polymer) and densification

To obtain the ZrC/polymer mixture, different proportions of ZrC/(0-20wt% SiC) were tested. The liquid preceramic polymer was directly mixed with the milled ZrC powders in toluene solvent, and then stirred for 24 hours at room temperature. At the end, the mixtures were dried in a rotary evaporator. The whole process is presented in Fig.1.

After the evaporation, the composite systems were poured into a graphite die with an inner diameter of 13 mm, and finally densified under vacuum following an optimized treatment by Spark Plasma Sintering (Syntex, Japan, Dr.Sinter 825).

2.4. Characterization

2.4.1. Synthesized ZrC powders

The global oxygen and carbon content were measured by Instrumental Gas Analysis (IGA) using EMIA 820V for carbon and EMGA 620W for oxygen. For each analysis, $CO_{(g)}$ and $CO_{2(g)}$ released after the combustion of the powders were quantified by IR measurements. These measurements were performed in an alumina or a graphite crucible for the carbon and oxygen analyses,

respectively. The calibration was achieved by steel standards containing well known carbon and oxygen contents. Zirconium content (mass percentage) was calculated taking into account the mass percentage of oxygen and the carbon obtained experimentally and using the principle of mass conservation for a composition ZrC_xO_y ($Zr_{(wt\%)} = 100 - C_{(wt\%)} - O_{(wt\%)}$). The oxycarbide powders were analyzed by X-ray diffraction with $CuK_{\alpha 1,2}$ and radiations using *LYNXEYE XE-T* detector (D8 advance, Bruker, Wissembourg, France) for angles (2θ) ranging between 20° and 120° (step: 0.02°, step time: 0.3 s) to identify the crystallized phases. Scanning electron microscopy (JSM - IT300 LV, Japon) and transmission electron microscopy (JEOL - 2100F, Tokyo, Japan) characterizations were carried out to observe the morphology of the synthesized oxycarbide powders. The size distribution of the powder before and after attrition milling was determined by laser granulometry (Horiba LA950, Kyoto, Japan).

2.4.2. Polymer (SMP-10)

Elemental analyses (C, H, O) of the polymer were investigated using a Flash EA 1112 (Thermo Finnigan). The structural characterizations of the polymer were carried out using different techniques. Attenuated Total Reflectance infra-Red spectroscopy (Nicolet IS10, Thermo Scientific, logiciel Omnic), in transmittance mode (4000-400 cm^{-1}) was performed. ^{29}Si liquid-state NMR spectra were recorded at 99 MHz on a Bruker Advance 500 spectrometer with a number of scans of 12288 and a relaxation time of 5 seconds. ^{29}Si Solid-state NMR was used to characterize the pyrolyzed polymer (1400 °C). The spectra were recorded at 139 MHz on a Bruker Avance 700 spectrometer with a number of scans of 456 and a relaxation time of 120 seconds. For both analyzes, chemical shifts were

referenced to tetramethylsilane (δ = 0 ppm). The thermal behavior was studied by a thermogravimetric analyzer (STA 449F3-Netzsch) coupled with a mass spectrometer (Omnistar, Balzers Instrument) following these experimental conditions: maximum temperature: 1400 °C, argon flow: 20 mL.min^{-1}, heating rate: 10 °C.min^{-1}.

2.4.3. Mixture (ZrC/polymer)

X-ray photoelectron spectroscopy (XPS, Kratos Axis Ultra DLD spectrometer) was used to highlight the presence of the polymer on the surface. A monochromatic AlKα source (15 mA, 15 kV) was utilized. All binding energy scales were recalibrated so that the C_{1s} peak arising from surface contamination is placed at 285.0 eV. The pass energy was 20 and 160 eV for the high-resolution spectra.

2.4.4. Densified composites

Phase identification and distribution of the composites were analyzed by XRD and SEM following the same parameters applied to the synthesized ZrC powders. Densities were determined using the Archimedes method with deionized water. Apparent elastic constants (Young's modulus, shear modulus) were determined by ultrasonic method using 10MHz transductors working in reflexion mode (WC37-10 and SW37 10,Ultran,State College, USA) on 2 mm thick samples. Vickers hardness was determined by microhardness tester (Micromet 6040, Buehler, USA) under a load of 100 g and dwell time of 10 s.

3. Results and discussion

3.1. Chemical composition and morphology of ZrC powders

Firstly, XRD analysis (fig.2.a) highlighted the presence of the characteristic peaks of a single-phased XRD pattern that can be indexed to zirconium carbide (PDF file 00-035-0784). Residual zirconia or carbon black were not detected, which confirmed a complete reaction between these two reagents. It was therefore necessary to determine accurately the chemical composition of the synthesized powders.

The samples were globally analyzed by elemental analyses. The results reported in Tab.1 stated out a composition of $ZrC_{0.90}O_{0.10}$ for the synthesized powders with a good correlation between the oxygen and carbon amounts. Zirconium carbide being a sub-stoichiometric carbon compound, it has a solubility limit between $ZrC_{0.55}$ and $ZrC_{0.98}$. In addition, the size of the oxygen being close to that of carbon, it can be introduced into the crystal lattice of the carbide forming a solid solution ZrC_xO_y. The results obtained in this study were in good agreement with the elemental analysis of Réjasse *et al*. [15] for the same composition. The authors explained that the amount of detected oxygen may come from the oxygen incorporated into the zirconium oxycarbide crystal lattice since crystallized zirconia was not detected by XRD. The amount of carbon may represent the contribution of both structural carbon incorporated within the oxycarbide lattice and the unreacted free carbon.

The authors suggested also that TEM is a powerful tool to investigate the presence of free carbon in the oxycarbide powders. Indeed, due to the molar mass of carbon, a slight molar excess leads to a large volume proportion, which is easily detected by TEM observations. Referring to the TEM image (fig.3.a),

the synthesized powders did not show any excess of carbon. The particles displayed an agglomeration tendency forming aggregates with a diameter ranging from 400 to 700 nm.

Moreover, SEM characterization confirmed a coalescence of the particles (fig.3.b). The presence of these agglomerates could be detrimental to the sintering of the composites. Indeed, a preferential sintering of the agglomerates (which may contain porosity) instead of elementary particles is likely to limit the densification of the composites. The objective was therefore to reduce the size of these agglomerates in order to improve the sinterability and the powder impregnation by the polymer. Among the various ball-milling techniques, attrition was performed following an optimized milling cycle. According to fig.3.c, raw ZrC powders had a monomodal size distribution centered at 3.5 µm. After the milling, the average diameter of the agglomerates decreased to reach 1.7 µm. As a result of strong shearing forces applied by the micrometric milling beads, the optimized milling cycle proved to be efficient in dispersing the initial agglomerates into smaller agglomerated particles with a monomodal size distribution centered at 1.7 µm. After controlling the quality of the synthesized ZrC powders in terms of chemical composition and particle size, the thermal behavior and the chemical composition of the commercial polymer (SMP-10) were studied. This thermal behavior will be taken into account to optimize the sintering of the hybrid systems.

3.2. Structural characterizations and thermal behavior of the polymer

The structure/composition of the polymer influences the chemical composition of the final ceramic and therefore its physico-chemical properties [16]. To elucidate the SMP-10 composition, elemental analysis was used. It can be seen from Tab.1

that the experimental composition is almost free of oxygen (< 0.05wt%) with a chemical formula near to the theoretical formula presented in literature ($SiC_{1.33}H_{4.4}$) [17]. Once the chemical composition and the structure of raw SMP-10 (fig.S1 and fig.S2a) were verified, it was necessary to investigate its thermal behavior. For this, SMP-10 was analyzed by TGA/MS at 1400 °C. TGA/MS curves showed three domains of mass loss (fig.4). The first step started at 100 °C and indicated a mass loss of 10%. Li *et al.*[18] stated out that at this temperature range, the evaporation of small oligomers is considered to be the main reason for weight loss. This assumption was confirmed by the MS spectra, which did not show any fragmentation of molecules (H_2 or CH_4). The second step began at 400 °C and displayed a mass loss of 14%, caused by the volatilization of fragments such as m/z = 2 (H_2) and m/z = 16 (CH_4). These fragments were detected by Li *et al.*[18] and Yu *et al.*[19], and attributed to the dehydrocoupling reactions and decomposition of the organic groups, which indicate the beginning of the polymer-to-ceramic conversion. At the beginning of 600 °C, a low mass loss (3%) was observed accompanied also with the volatilization of m/z = 2 (H_2), m/z = 16 (CH_4) and also fragment with higher molecular weight m/z = 44 (C_3H_8). This feature represented the final stage of the polymer-to-ceramic conversion. Beyond 800 °C, no significant mass loss was recorded, indicating a complete polymer-to-ceramic conversion with a ceramic yield of 73%. It should be noted that these gaseous species represent a critical parameter to be considered during the sintering optimization. Indeed, microstructural defects may be generated by the release of gaseous species during sintering.

Furthermore, the heat treated SMP-10 were characterized by solid-state NMR ^{29}Si and XRD. The NMR spectra (fig.S2.b) showed a single chemical shift at -15 ppm, which reflected the single environment of the silicon in the cubic form of silicon carbide (β-SiC) [20]. To complete this analysis, the XRD diagram confirmed the presence of broad peaks associated to a nanocristallized β-SiC phase (fig.2.b).

3.3. Morphological and chemical characterizations of the mixtures ZrC/polymer

Once the powder was synthesized and the polymer characterized, both were mixed according to the protocol presented previously. The aim of this step of the process was to prepare powder/polymer mixtures where the polymer would be well dispersed in the mixture and would homogeneously coat the ZrC particles. This could favor the homogeneity of the final material. Indeed, after the evaporation, two textures were obtained (fig.S3). The compositions were calculated as a function of the equivalent mass percentage of SiC obtained after the heat treatment of the polymer. The compositions with a wt%SiC less than 10% had a pulverulent aspect while the composites with a wt%SiC higher than 10% displayed a viscous aspect (fig.S3). The samples with more than 10wt% of SiC were unsuitable for being sintered by SPS because of the leakage of matter when applying pressure. During this work, we concentrated only on the study of ZrC/(10wt%SiC) composition.

First, TEM analyses were used to investigate the morphology of zirconium carbide powder and the mixture ZrC/polymer at the nanometric scale. According to the images, ZrC particles presented a thin layer at the surface with a thickness

of 3 nm (fig.5.a). This layer is generally present in carbides and can be attributed to oxides phases [21]. In fig.5.b, a second amorphous layer appeared with a thickness ranging from 5 to 10 nm, likely due to the commercial polymer SMP-10.

To determine the surface composition of the mixture, a further XPS study was performed to define the nature of the bonds present on the surface. Among the detected elements (C, O, Si, Zr), the spectral zones of silicon and zirconium were presented.

For ZrC powders (fig.6.a), the deconvolution of the Zr_{3d} peak showed four contributions. The two lowest binding energy peaks (179.51 eV, 181.94 eV) can be attributed to Zr-C bonds and can be assigned to zirconium carbide, while the two highest bending energy peaks (182.59 eV, 185.02 eV) correspond to Zr-O bonds and can be attributed to amorphous zirconia. These results are consistent with the work of Chu *et al.*[22] and Lucas *et al.*[23], and confirm the presence of an oxide layer onto the synthesized powders surface. The presence of the polymer was confirmed from the Si_{2p} spectrum (fig.6.b). The deconvolution of the Si_{2p} peak indicated two contributions at 101.46 and 102.59 eV. These peaks were located slightly far from the binding energy usually obtained from Si-C bonds in stoichiometric silicon carbide (100.5 eV) [24] and were assigned to Si-C bonds that belong to an O_x-Si-C_y environments (fig.7.b). These results were in good agreement with XPS analyses of previous works [25] where an hydrolyzed AHPCS film was analyzed. It is worth adding that since our polymer did not have any oxygen inside its structure (Tab.1), the presence of O_x-Si-C_y environments

may be related to a possible reaction between either the zirconia layer or the adsorbed water and the hydrogenosilane functions of the polymer [26].

3.4. Densification of the mixtures ZrC/polymer

Due to the presence of polymer in our mixtures, our optimization was firstly focused on the determination of a temperature that will promote the conversion of the polymer prior to sintering. Relying on the TGA results, which showed a mass loss up to 800 °C (fig.4), three temperatures were chosen, *i.e.* 600,700 and 800 °C. During sintering, the temperature was measured by the pyrometer on the die surface, which is largely underestimates the actual temperature of the sample [27]. This optimization was carried out using a fixed dwell time of 10 minutes and a pressure of 25 MPa. The latter was then increased at the end of the dwell time to reach 75 MPa.

SPS conditions for the sintering step were then fixed with dwell time of 5 min, a heating rate of 200 °C/min and a pressure of 75 MPa, under vacuum. The maximum temperature was fixed at 1950 °C according to anterior studies [12].

The evolution of the gas pressure in the SPS chamber and of the associated thermal treatment as a function of the time was plotted (fig.7). Three different degassing steps, characterized by a peak in the pressure, were highlighted depending on the dwell temperature. The first peaks presented a high gas release at a temperature lower than the pyrometer detection (<573°C). This was due to the release of gaseous species caused during the conversion of the polymer into ceramics. The first step showed a less pronouncing degassing for the test conducted at 600 °C. The second step, which occurred when the heating up restarted, may be caused by the release of gaseous species resulting from the

first step and that have condensed on the coldest areas of the SPS system, or it can be associated with the end of organic-inorganic conversion. It is also worth mentioning that the degassing at 600 °C was higher indicating that the release of gaseous species might still occur at this stage. Finally, the third step may correspond to an *in-situ* carboreduction of the oxide layer, which was often observed in the sintering of carbides [28].

As a result of this first optimization, different microstructures were obtained. The three microstructures presented a well homogenous distribution of the SiC phase into the ZrC matrix (fig.8). Nevertheless, residual porosity was present in the microstructures. Indeed, the use of a dwell temperature of 600 °C (fig.8.a) was not sufficient to promote a complete departure of volatile fragments. It is possible that some organic species remained trapped in the structure, and left as heating up restarted (fig.8.a). This was consistent with the degassing curve at 600 °C, which showed a higher gas release at the beginning of step 2. Nevertheless, the increase of the applied pressure until 75 MPa at the beginning of step 2 may cause entrapment of gas from the organic species, and thus, generating porosity after sintering. A dwell temperature of 800 °C displayed a more porous microstructure (fig.8.c). Indeed, the higher dwell temperature would cause a brutal removal of organic species generating microstructural defects with larger porosity (fig.8.c). These differences were also observed by looking at the open porosity and the density (tab.3). Interrupted tests, before heating up restarts, were also performed at the three temperatures in order to analyze the morphology of the mixtures after the conversion step (fig. S5). For either manually interrupted or completed tests, the conversion at 800 °C led to higher open porosities (tab.3).

In addition, the impact on the density clearly identified the dwell temperature of 700 °C as the best choice in the conversion route from organic to ceramic. It should also be noted that the pellets obtained with this dwell temperature broke during polishing, unlike the ones sintered using 600 and 700 °C dwell temperature, respectively. Finally, the microstructure obtained using a conversion temperature of 700 °C displayed a good compromise between porosity and homogeneity (fig.8.b and fig.S5). Indeed, the latter showed less porosity compared with the two other microstructures. It seemed that the use of a conversion temperature of 700 ° C promoted the total conversion of the polymer while avoiding the formation of microstructural defects generated by a brutal departure of organic species. For this, this conversion temperature was selected for the following tests.

Once the dwell temperature for the polymer to ceramic conversion was figured out, the optimization of the maximum sintering temperature was required in order to promote the removal of the remained porosity. For this, interrupting tests were performed from room temperature to 1950 °C in order to investigate the evolution of the microstructure during sintering. Each test was preceded by a dwell temperature of 700 °C for 10 minutes to promote the polymer to ceramic conversion prior to sintering.

The evolution of the displacement and the temperature as a function of time as well as the evolution of the microstructure at different steps of the sintering were studied (fig.9). At room temperature, the microstructure showed ZrC particles coated with polymer. It was then converted during the first dwell time, and appeared to maintain the particles linked to each other (800 °C). It was also

noticed that the particle size of ZrC (D_m< 1µm) did not change during the conversion of the polymer and the pellet was cohesive after the interrupted test. The increase of the displacement was detected right before the heating restarted up. It was associated to the increase of the pressure from 25 to 75 MPa. By the beginning of the sintering around 1550 °C (confirmed by the increase of the displacement), the open porosity started to decrease. These first three temperatures (25, 800 and 1550 °C) represented the first step of sintering, which was manifested by the rearrangement and bridging between particles. Right after, the densification (increasing of the displacement) and the elimination of the open porosity occurred. Indeed, the open porosity decreased from 24 to 0.7% between 1550 and 1700 °C, respectively. The microstructure at this temperature showed a fine and homogenous phase distribution. By increasing the temperature until the end of the thermal treatment (1950 °C), step 3 of sintering occurred. Indeed, it was manifested by a coarsening of the SiC phase (black particles) and a growth of porosity (especially closed porosity), which was detrimental to densification [29]. Following these results, it seemed that the use of the optimized dwell temperature (700 °C) followed by a sintering at a maximum temperature of 1700 °C (without dwell time) offered a good compromise between obtaining a dense microstructure with a fine and homogeneous distribution of phases (fig.10). The estimated size of SiC domains is centered at 300 nm (estimated by Image J tool, fig.10.b).

3.5. Microstructure and mechanical properties of the sintered composites

After the optimization of the sintering cycle, the influence of SiC on the mechanical properties of ZrC were studied. For that, three samples of ZrC/ (0-

10wt%SiC) were sintered using the optimized sintering cycle with a dwell time of 5 minutes at 1700 °C.

On the one hand, from fig.11.b and tab.2, the addition of 5wt%SiC did not affect the densification of the ZrC monolith (fig.11.a) despite a decrease in the open porosity. On the other hand, the addition of 10wt%SiC (fig.11.c) offered a well homogenous and fine microstructure of SiC phases. Indeed, a sample with an undetectable open porosity and a relative density of 97% was obtained. As a result, it appears that increasing the SiC content improve the densification. The relative density increased from 93.4 to 97.1% for a ZrC monolith and a ZrC / 10wt% SiC composite, respectively. The improvement of the densification may be due to the homogenous distribution of SiC particles at grain boundaries and thus inhibiting grain growth of ZrC. It is possible also that the use of the preceramic polymer has a positive impact on the densification by improving rearrangement between particles during the first step of sintering. Regarding the mechanical properties, the addition of the SiC retained the elastic constants of the ZrC monolith. For a composition of ZrC /10wt%SiC, the elastic constants reported by Lucas *et al.*[12] are pretty close to the one obtained in this study. For the Vickers hardness, the reported values were quite close to those reported by Sagdic *et al.*[8] but lower than the Vickers hardness of both monolith ZrC and SiC (Hv > 20 GPa) [30].

4. Conclusion

During this work, a promising route was employed to manufacture ZrC/SiC composites using PDC route and Spark Plasma Sintering. The originality of this work consists in the direct ceramization/sintering of a ZrC/polymer mixture without any previous crosslinking steps. For that, a control of the quality of the synthesized powders (chemical composition and particle size) and an optimization of the sintering parameters were required. The original process used in this study gave access to fabricate composites with a well fine and homogenous phase distribution and good mechanical properties at relatively low temperature (1700 °C) compared to the high temperature required for the sintering of this refractory composites. The influence of the addition of SiC (up to 10wt%) was studied and related to the final relative densities and mechanical properties of the composites. The main following conclusions can be issued from the obtained results:

- TEM analysis has demonstrated the presence of two layers on the surface of the mixture, one associated with the oxide layer and the other with the preceramic polymer. This would be beneficial for a potential fabrication of core-shell systems;
- The optimization of sintering parameters revealed that a dwell time of 10 minutes at 700 °C was essential to promote a conversion of the polymer into ceramics, followed by a treatment at 1700 °C for 5 minutes to fully densify the composites;

- The addition of 10 wt%SiC increased the relative density from 93.4 to 97.1% and a well homogenous phase distribution with fine SiC domains (300 nm) was achieved;
- Finally, it has been shown that the addition of the SiC slightly increase the elastic constants of the ZrC monolith and does not affect its Vickers hardness. The apparent Young modulus, shear modulus and Vickers hardness were 402 GPa, 166 GPa, and 15.9 GPa respectively for the ZrC/ 10wt%SiC.

References

1. Paton NE. Materials for advanced space propulsion systems. Mater Sci Eng A, 1991. p. 21–29.
2. Borrelli R, Riccio A, Tescione D, Gardi R, Marino G. Thermo-structural behaviour of an UHTC made nose cap of a reentry vehicle. Acta Astronaut, 2009. p. 442–456.
3. Xie W, Peng Z, Meng S, Xu C, Yi F, Jin H, et al. Thermal stress analysis of the FGLCS in hypersonic vehicles: Their application to fuel injection struts in scramjets. Compos Part Appl Sci Manuf, 2017. p. 157–165.
4. Kral C, Lengauer W, Rafaja D, Ettmayer P. Critical review on the elastic properties of transition metal carbides, nitrides and carbonitrides. J Alloys Compd, 1998. p. 215–233.
5. Shimada S, Ishil T. Oxidation Kinetics of Zirconium Carbide at Relatively Low Temperatures. J Am Ceram Soc, 1990. p. 2804–2808.
6. Pizon D, Charpentier L, Lucas R, Foucaud S, Maître A, Balat-Pichelin M. Oxidation behavior of spark plasma sintered ZrC–SiC composites obtained from the polymer-derived ceramics route. Ceram Int, 2014. p. 5025–5031.
7. Zhao L, Jia D, Duan X, Yang Z, Zhou Y. Pressureless sintering of ZrC-based ceramics by enhancing powder sinterability. Int J Refract Met Hard Mater, 2011. p. 516–521.
8. Sagdic S, Akin I, Sahin F, Yucel O. Mechanical Properties of Spark Plasma Sintered ZrC-SiC Composites. TMS Annual Meeting, 2012. p. 569-575.
9. Bao X, Edirisinghe MohanJ. Different strategies for the synthesis of silicon carbide–silicon nitride composites from preceramic polymers. Compos Part Appl Sci Manuf, 1999. p. 601–610.

10. Chen S, Zhang C, Zhang Y, Zhao D, Hu H, Xiong X. Effects of polymer derived SiC interphase on the properties of C/ZrC composites. Mater Des, 2014. p. 102–107.
11. Jones R, Szweda A, Petrak D. Polymer derived ceramic matrix composites. Compos Part Appl Sci Manuf, 1999. p. 569–575.
12. Lucas R, Davis CE, Clegg WJ, Pizon D, Babonneau F, Foucaud S, et al. Elaboration of ZrC-SiC composites by spark plasma sintering using polymer-derived ceramics. Ceram Int, 2014. p. 15703–15709.
13. Gendre M, Maître A, Trolliard G. Synthesis of zirconium oxycarbide (ZrCxOy) powders: Influence of stoichiometry on densification kinetics during spark plasma sintering and on mechanical properties. J Eur Ceram Soc, 2011. p. 2377–2385.
14. Seo M, Kang S, Kim Y, Ryu S-S. Preparation of highly dispersed ultra-fine ZrC by combination of carbothermal reduction of ball-milled ZrO2 and C mixture and bead milling. ResearchGate, 2013. p. 345–350.
15. Réjasse F, Rapaud O, Trolliard G, Masson O, Maître A. Experimental investigation and thermodynamic evaluation of the C–O–Zr ternary system. RSC Adv 2016. p. 100122–100135.
16. Colombo P, Mera G, Riedel R, Sorarù GD. Polymer-Derived Ceramics: 40 Years of Research and Innovation in Advanced Ceramics. J Am Ceram Soc, 2010. p. 1805–1837.
17. Kaur S, Riedel R, Ionescu E. Pressureless fabrication of dense monolithic SiC ceramics from a polycarbosilane. J Eur Ceram Soc, 2014. p. 3571–3578.

18. Li H, Zhang L, Cheng L, Wang Y, Yu Z, Huang M, et al. Effect of the polycarbosilane structure on its final ceramic yield. J Eur Ceram Soc, 2008. p. 887–891.
19. Yu Z, Zhang P, Feng Y, Li S, Pei Y. Template-Free Synthesis of Porous Fe3O4/SiOC(H) Nanocomposites with Enhanced Catalytic Activity. J Am Ceram Soc, 2016. p. 2615–2624.
20. Finlay GR, Hartman JS, Richardson MF, Williams BL. 29 Si and 13C magic angle spinning n.m.r. spectra of silicon carbide polymorphs. J Chem Soc Chem Commun, 1985. p. 159–161.
21. Réjasse F, Georges M, Pradeilles N, Antou G, Maître A. Influence of chemical composition on mechanical properties of spark plasma sintered boron carbide monoliths. J Am Ceram Soc, 2018. p. 3767–3772.
22. Chu A, Qin M, Rafi-ud-din, Zhang L, Lu H, Jia B, et al. Carbothermal synthesis of ZrC powders using a combustion synthesis precursor. Int J Refract Met Hard Mater, 2013. p. 204–210.
23. Lucas R, Pizon D, Laborde E, Trolliard G, Foucaud S, Maître A. A simple route for organic covalent grafting onto zirconium carbide particles. Appl Surf Sci, 2013. p. 411–414.
24. Busiakiewicz A, Huczko A, Soszynski M, Polanski K, Maciej R, Klusek Z. Surface chemical composition of SiC-cored nanowires investigated at room and elevated temperatures in ultra-high vacuum. Vacuum, 2012. p. 1974–1978.

25. Li M, Kim DP. Silicate glass coated microchannels through a phase conversion process for glass-like electrokinetic performance. Lab Chip, 2011. p. 1126–1131.
26. Osei-Agyemang E, Paul JF, Lucas R, Foucaud S, Cristol S. Periodic DFT and Atomistic Thermodynamic Modeling of Reactivity of H2, O2, and H2O Molecules on Bare and Oxygen Modified ZrC (100) Surface. J Phys Chem. C, 2014. p. 12952–12961.
27. Antou G, Mathieu G, Trolliard G, Maître A. Spark plasma sintering of zirconium carbide and oxycarbide: Finite element modeling of current density, temperature, and stress distributions. J Mater Res, 2009. p. 404–412.
28. Georges M. Approche du frittage SPS de céramiques fines de carbure de bore : rôle des poudres initiales et de la mise en forme. thesis. Limoges, 2016.
29. German RM. Coarsening in Sintering: Grain Shape Distribution, Grain Size Distribution, and Grain Growth Kinetics in Solid-Pore Systems. Crit Rev Solid State Mater Sci, 2010. p. 263–305.
30. Pierson HO. Handbook of Refractory Carbides and Nitrides: Properties, Characteristics, Processing and Applications. William Andrew; 1996.

Fig.1. General process for the preparation of ZrC/SiC

Fig.2. XRD pattern of the synthesized ZrC powders a) and the heat-treated SMP-10 b)

Fig.3. TEM observation a) SEM image b) of the raw ZrC powders; c) Size distribution of the raw and the milled ZrC powders

Fig.4. TGA/MS of the commercial polymer SMP-10

Fig.5. TEM analyses of the zirconium carbide a), and the mixture ZrC/polymer

Fig.6. High resolution XPS spectra of Zr_{3d} of the synthesized powder a), and high resolution XPS spectra of Si_{2p} of the mixture b)

Fig.7. Evolution of gas pressure during sintering

Fig.8. SEM images of the mixtures sintered using a dwell temperature of 600 °C a) 700 °C b) and 800 °C c)

Fig.9. Evolution of the microstructure during sintering

Fig.10. SEM images of the sintered mixture following the optimized sintering cycle a) Estimated SiC domains size by ImageJ b)

Fig.11. SEM images of the polished surface of sintered ZrC monolith a) ZrC / 5wt%SiC b) and ZrC / 10wt%SiC c)

Samples	Elemental analysis					Calculated composition
	C (wt%)	O (wt%)	H (wt%)	Zr (wt%)	Si (wt%)	
Synthesized ZrC[1]	10.4 ± 0.2	1.5 ± 0.2	-	88.1	-	$ZrC_{0.90 \pm 0.02}O_{0.10 \pm 0,01}$
SMP-10[2]	33.1 ± 0.1	< 0.05	8.7 ± 0.1	-	58.2	$SiC_{1.33 \pm 0.01}H_{4.17 \pm 0,06}$

[1]: *measured by IGA*

[2]: *measured by Flash EA 1112*

Zr (wt%) and Si (wt%) : calculated using the principle of mass conservation

Tab.1. Elemental analysis of the synthesized ZrC powders and the raw SMP-10

Samples	Open porosity (%)	Young's modulus (GPa)	Shear modulus (GPa)	Vickers hardness (GPa)
100 ZrC	4	375 ± 2	155 ± 1	16.4 ± 1
ZrC / 5wt% SiC	0.3	401 ± 2	168 ± 1	16.3 ± 1
ZrC / 10wt% SiC	0	402 ± 2	166 ± 1	15.9 ± 1

Tab.2. Mechanical properties of the sintered samples

Samples	Interrupted tests		Completed tests		
	Open porosity (%)	Density (g/cm^3)	Open porosity (%)	Density (g/cm^3)	Relative density (%)
Conversion at 600 °C	33	3.70	< 1	6.09	97
Conversion at 700 °C	30	3.81	< 1	6.21	99
Conversion at 800 °C	36	3.72	2	6.08	97

Tab. 3: Open porosity and density measurements of ZrC/10wt% SiC samples obtained after the interrupted and complete tests, respectively

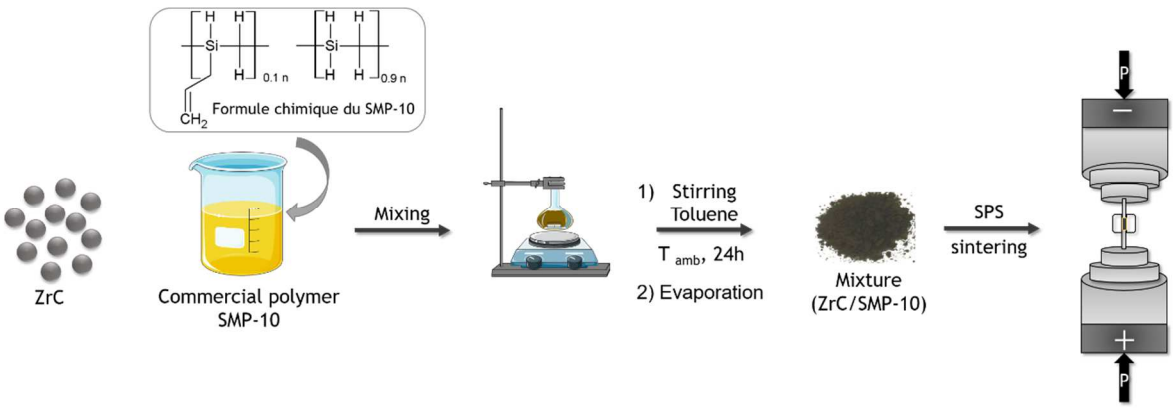

Fig.1. General process for the preparation of ZrC/SiC

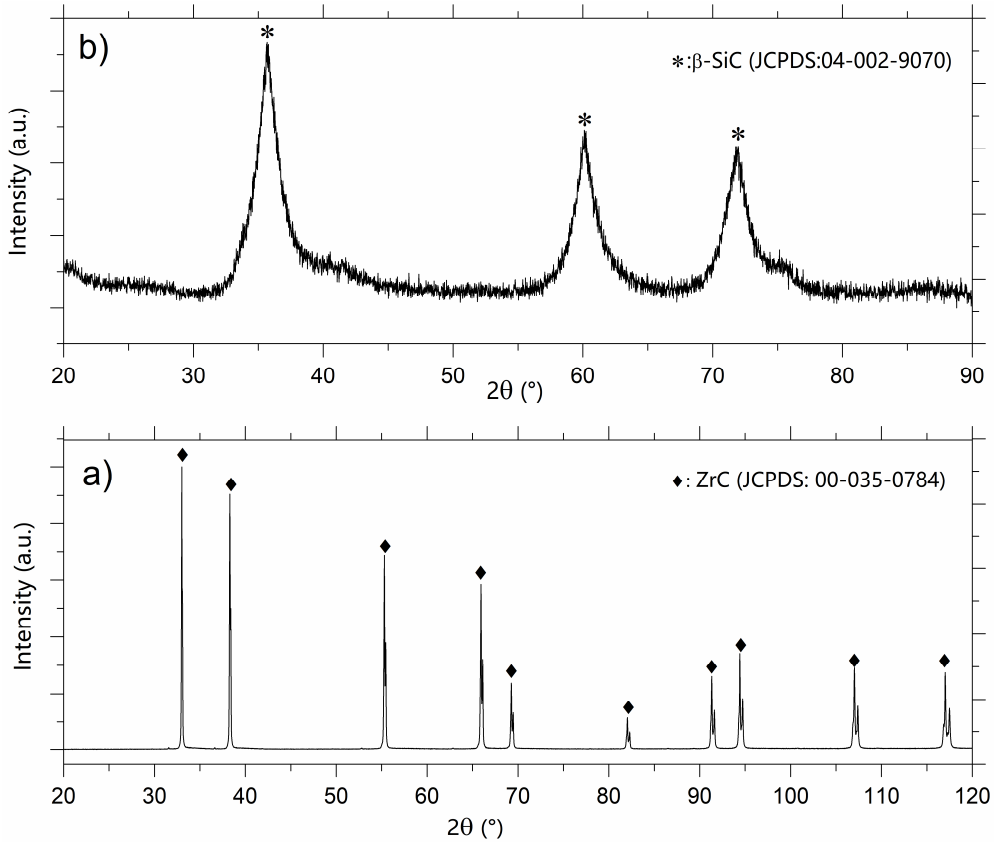

Fig.2. XRD pattern of the synthesized ZrC powders a) and the heat-treated SMP-10 b)

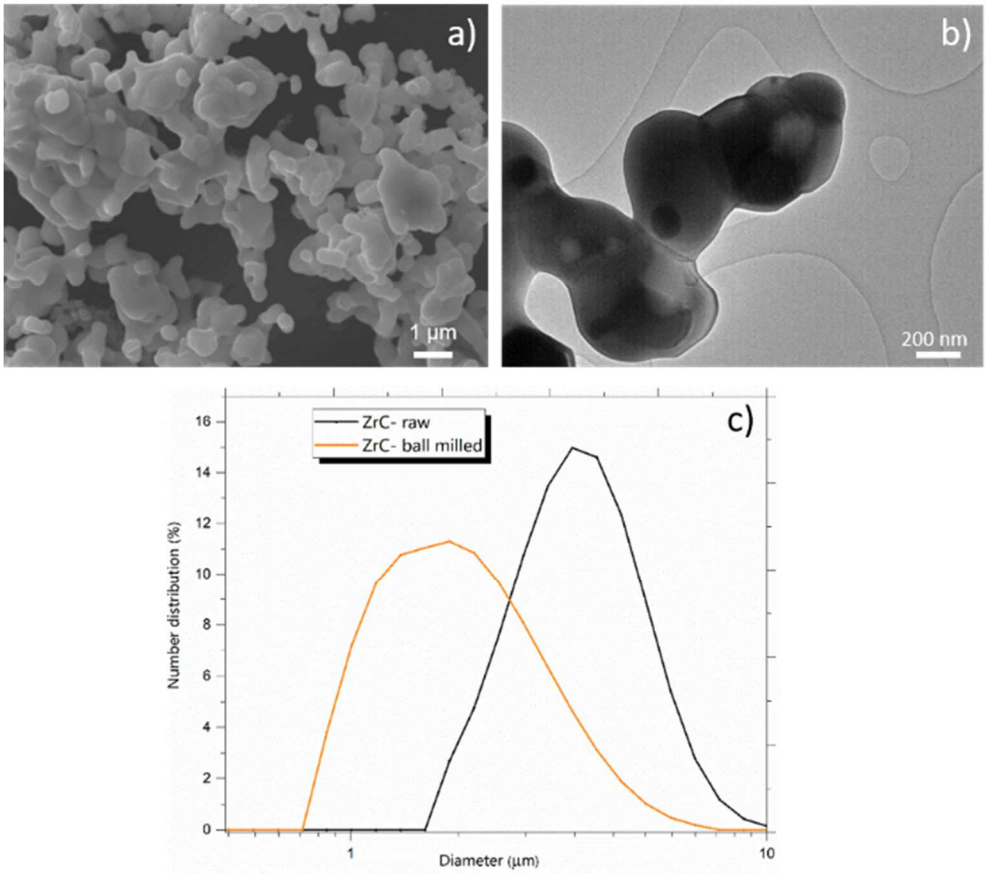

Fig.3. TEM observation a) SEM image b) of the raw ZrC powders; c) Size distribution of the raw and the milled ZrC powders

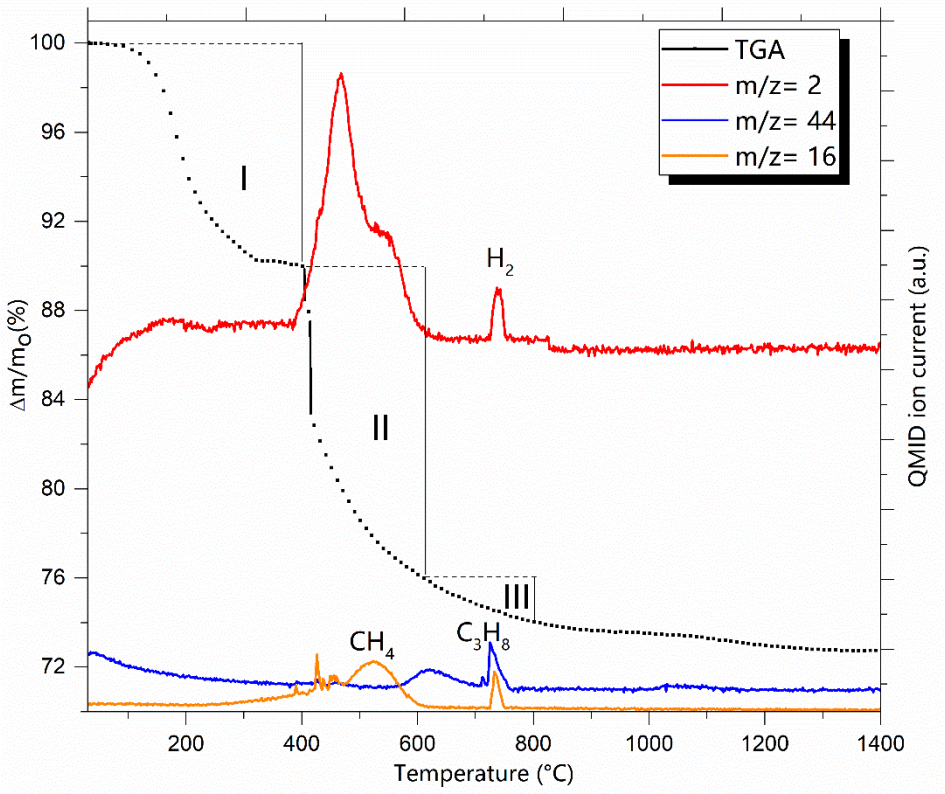

Fig.4. TGA/MS of the commercial polymer SMP-10

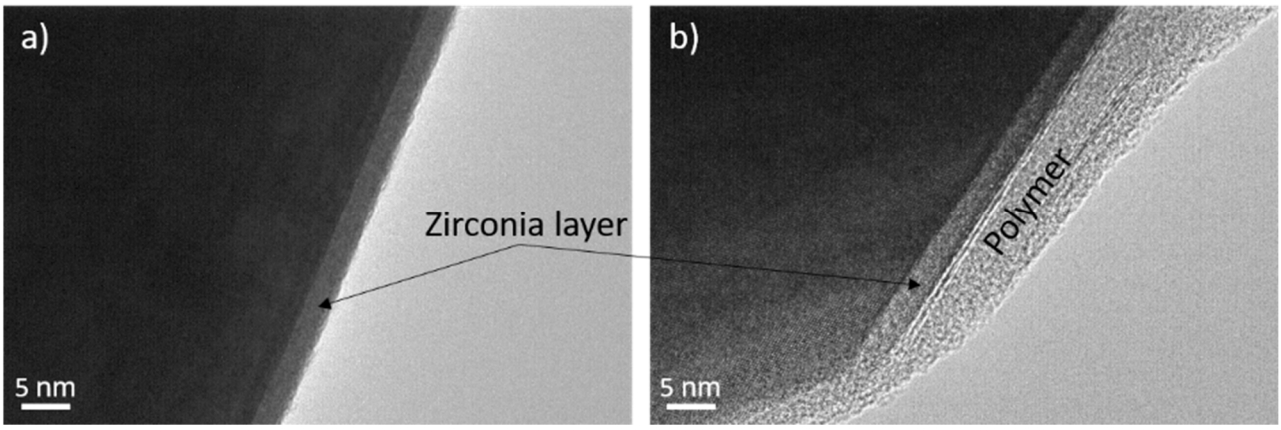

Fig.5. TEM analyses of the zirconium carbide a), and the mixture ZrC/polymer

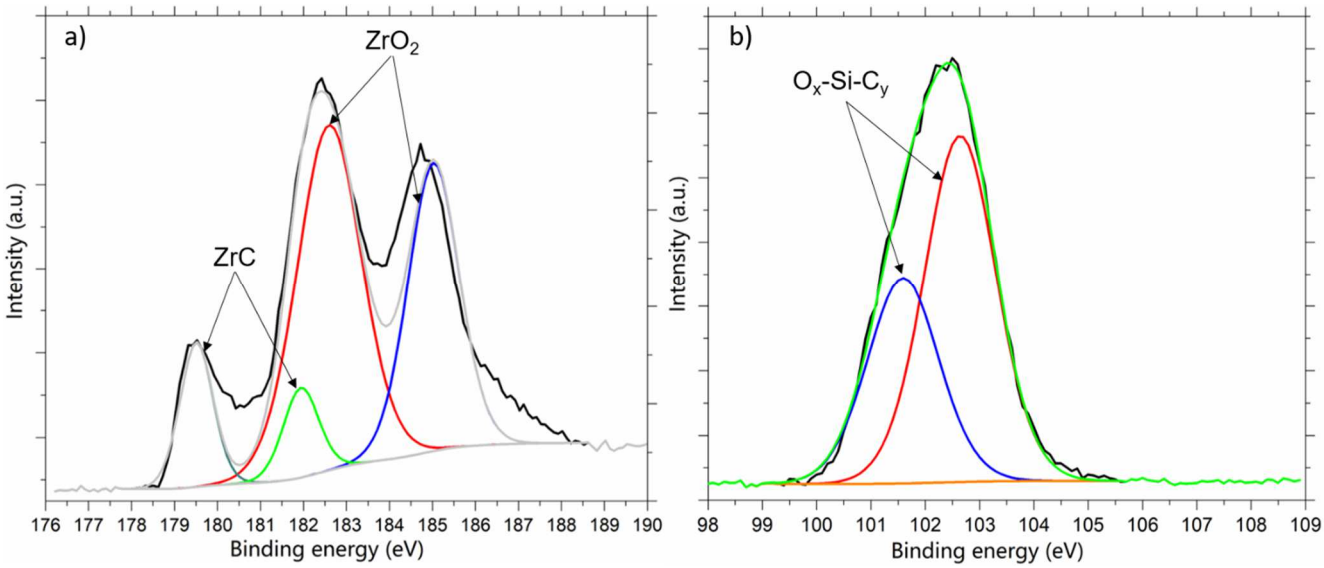

Fig.6. High resolution XPS spectra of Zr_{3d} of the synthesized powder a), and high resolution XPS spectra of Si_{2p} of the mixture b)

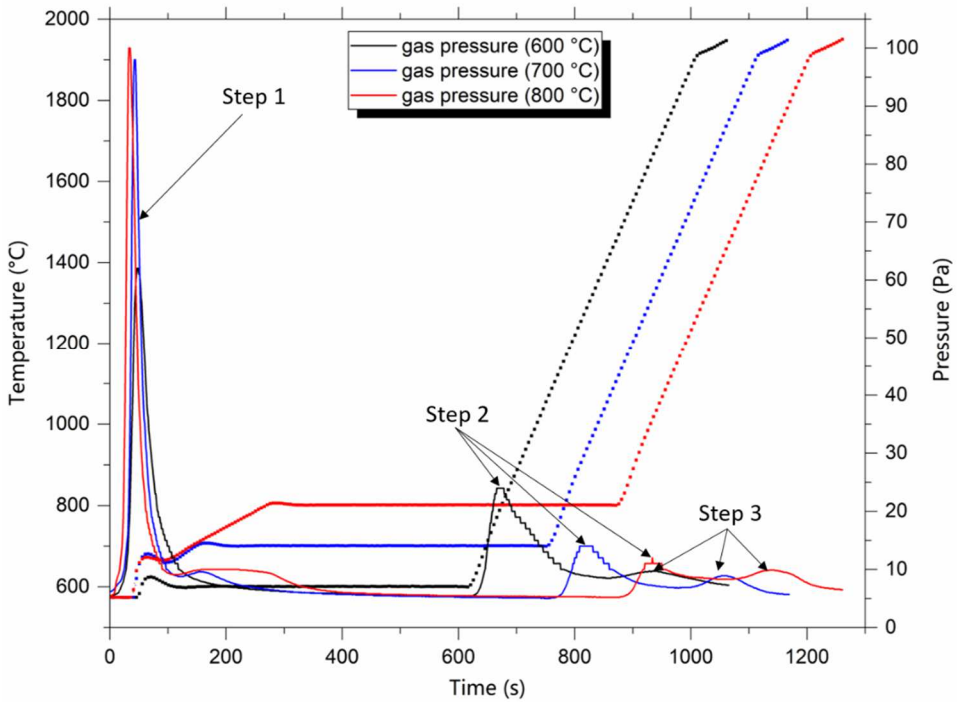

Fig.7. Evolution of gas pressure during sintering

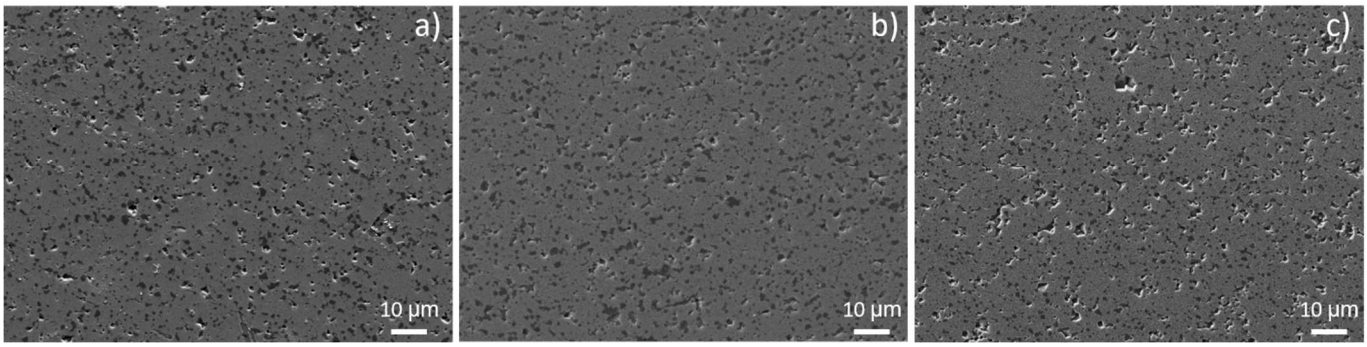

Fig.8. SEM images of the mixtures sintered using a dwell temperature of 600 °C a) 700 °C b) and 800 °C c)

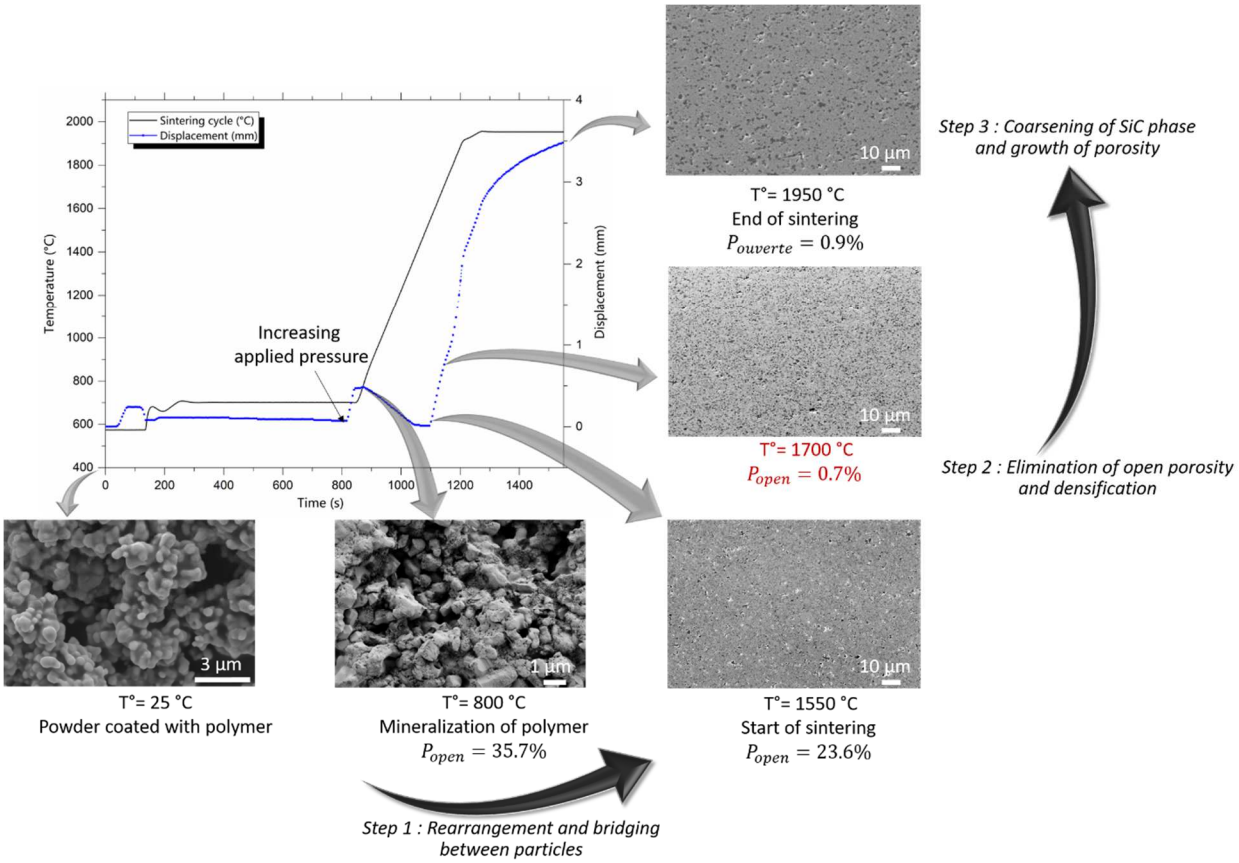

Fig.9. Evolution of the microstructure during sintering

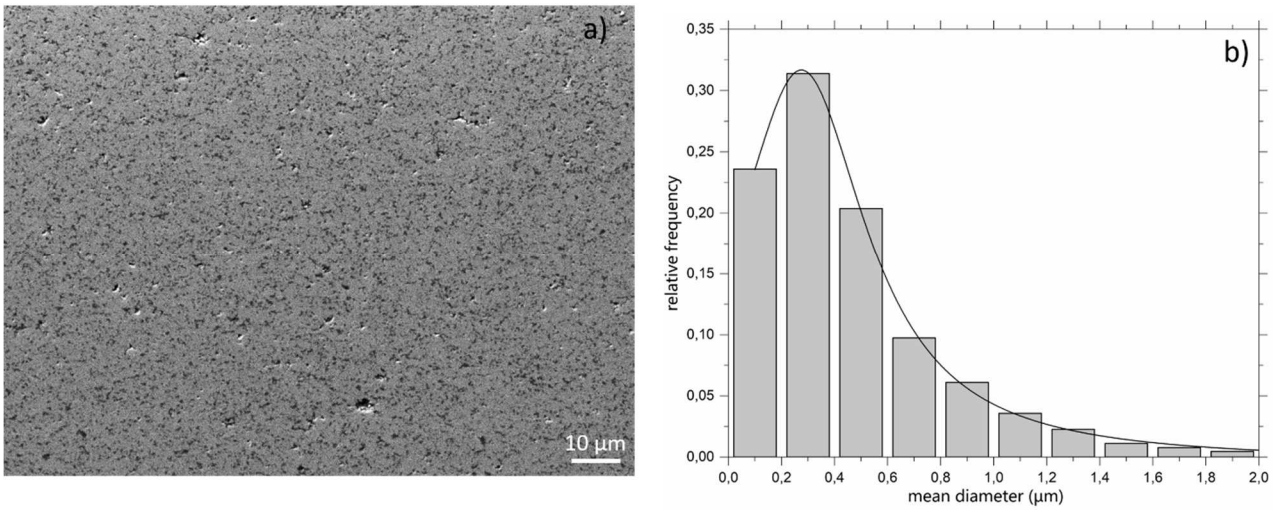

Fig.10. SEM images of the sintered mixture following the optimized sintering cycle a) Estimated SiC domains size by ImageJ b)

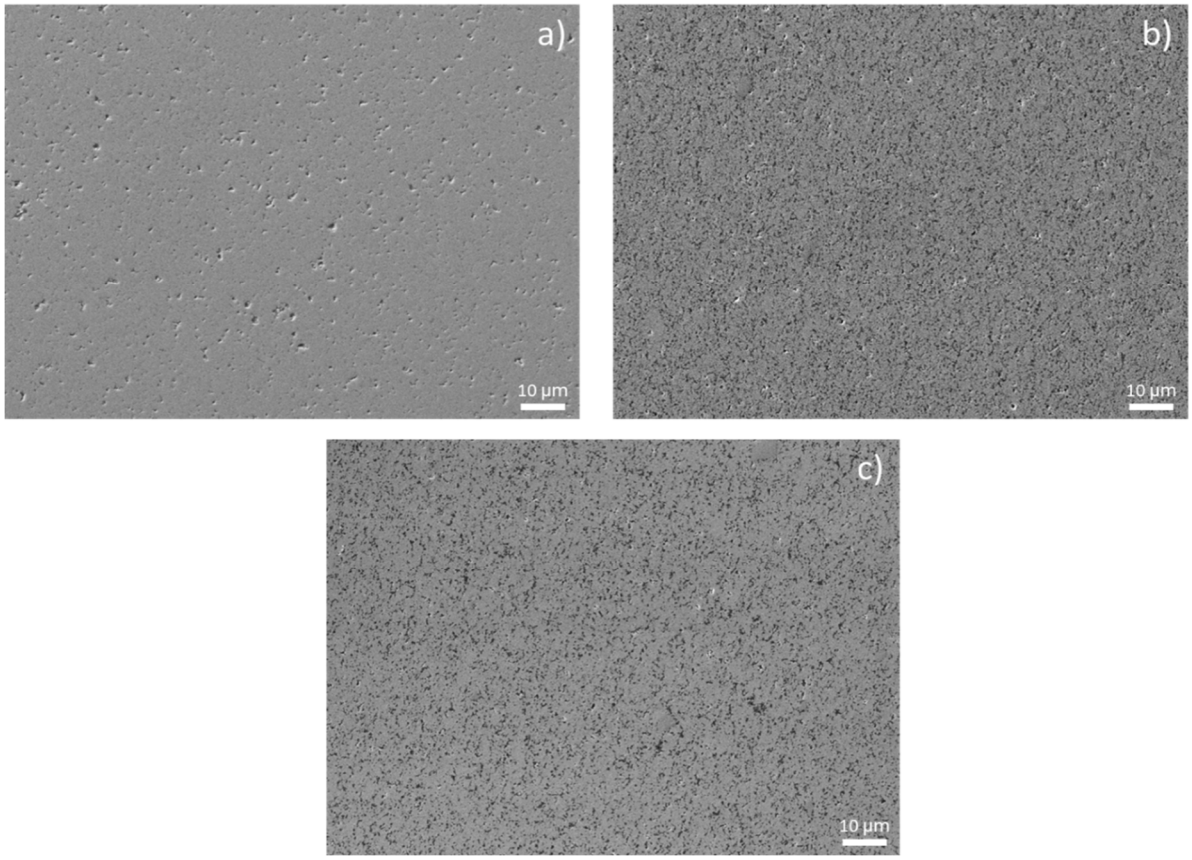

Fig.11. SEM images of the polished surface of sintered ZrC monolith a) ZrC / 5wt%SiC b) and ZrC / 10wt%SiC c)

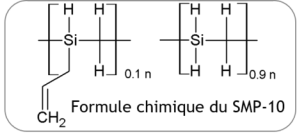

ZrC

Commercial polymer
SMP-10

Mixing

1) Stirring
Toluene

T_{amb}, 24h

2) Evaporation

Mixture
(ZrC/SMP-10)

SPS
sintering

P

P

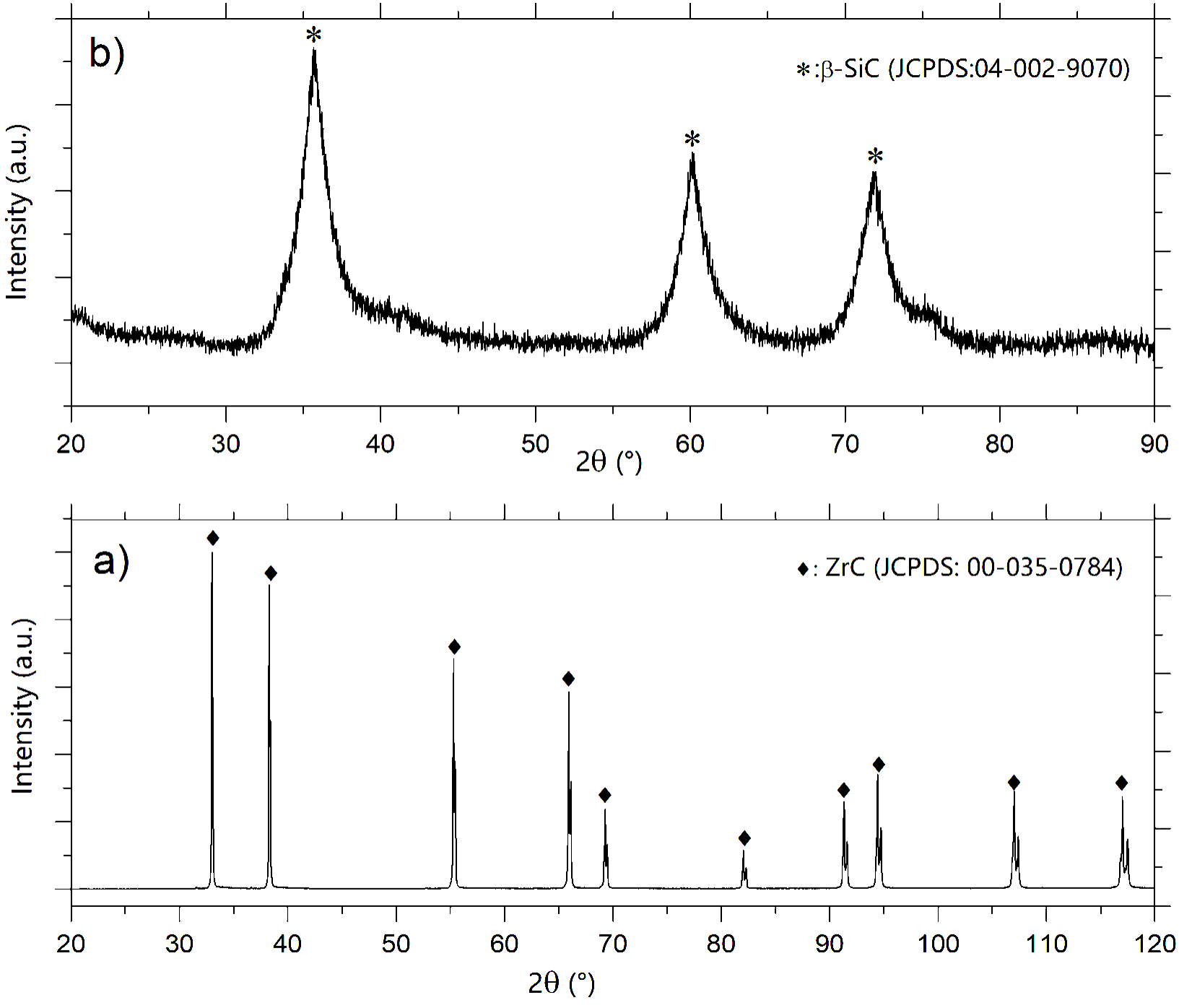
b)
*:β-SiC (JCPDS:04-002-9070)
Intensity (a.u.)
2θ (°)
20
30
40
50
60
70
80
90
a)
◆: ZrC (JCPDS: 00-035-0784)
Intensity (a.u.)
2θ (°)
20
30
40
50
60
70
80
90
100
110
120

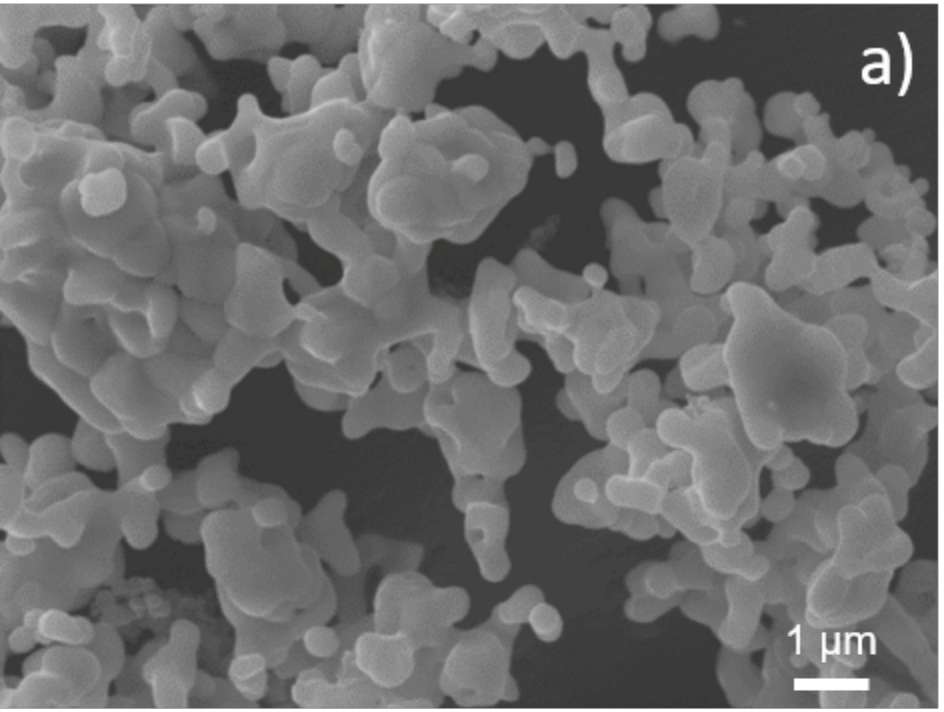
a)
1 µm

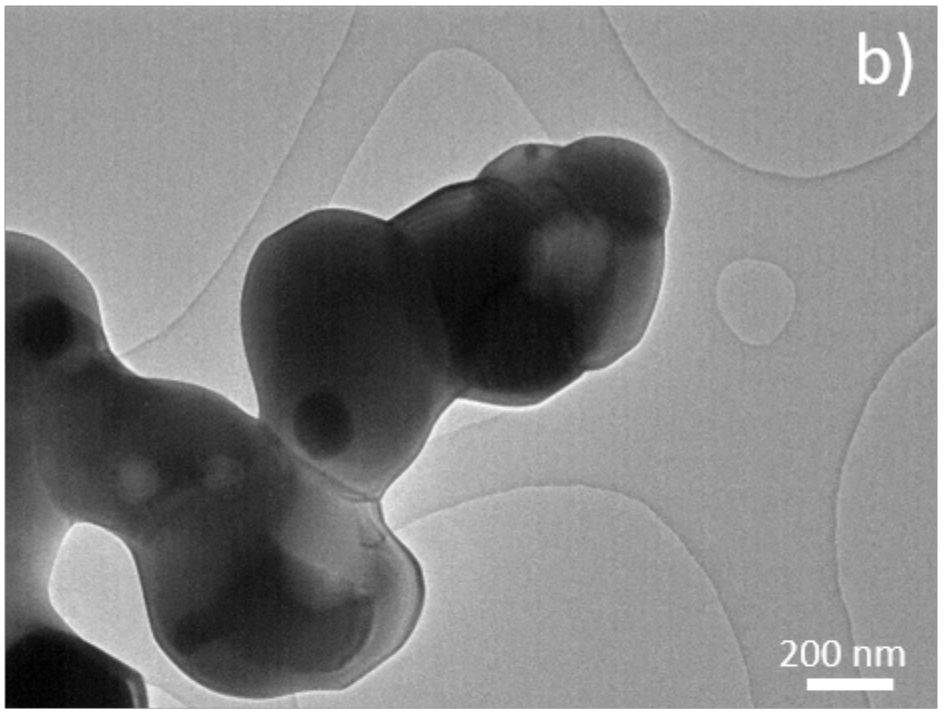
b)
200 nm

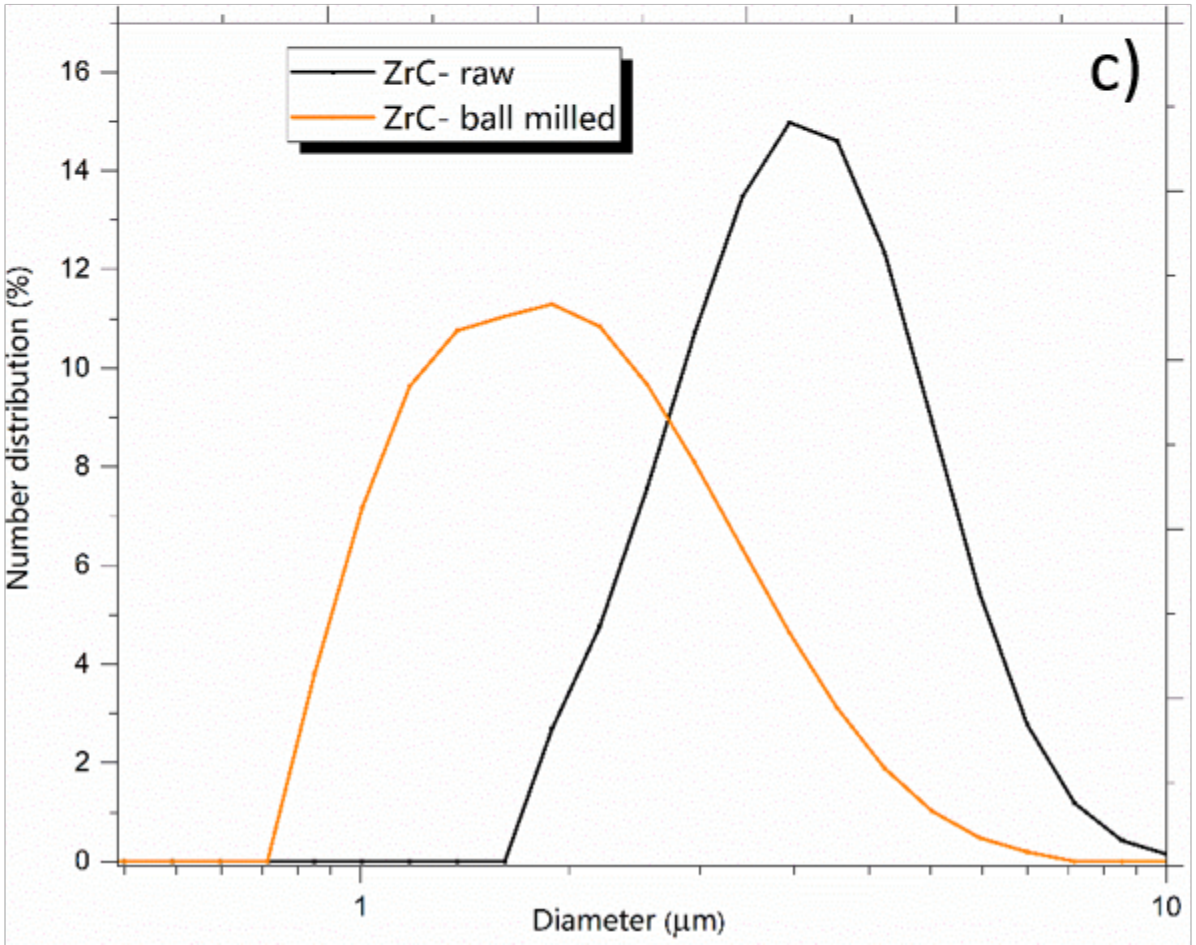
c)
ZrC- raw
ZrC- ball milled
Number distribution (%)
0
2
4
6
8
10
12
14
16
1
10
Diameter (µm)

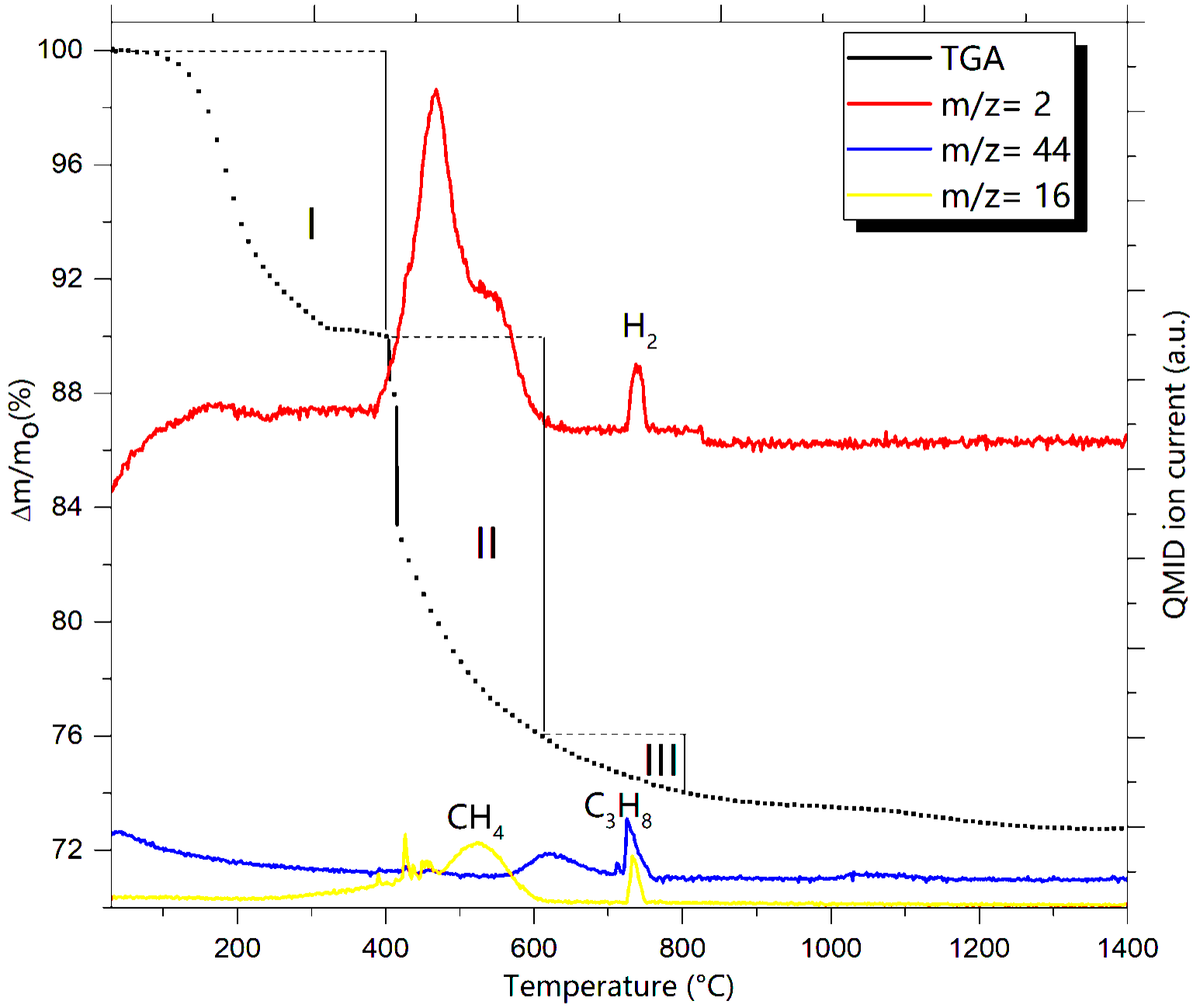
TGA
m/z= 2
m/z= 44
m/z= 16
I
II
III
H2
CH4
C3H8
100
96
92
88
84
80
76
72
Δm/mO(%)
200
400
600
800
1000
1200
1400
Temperature (°C)
QMID ion current (a.u.)

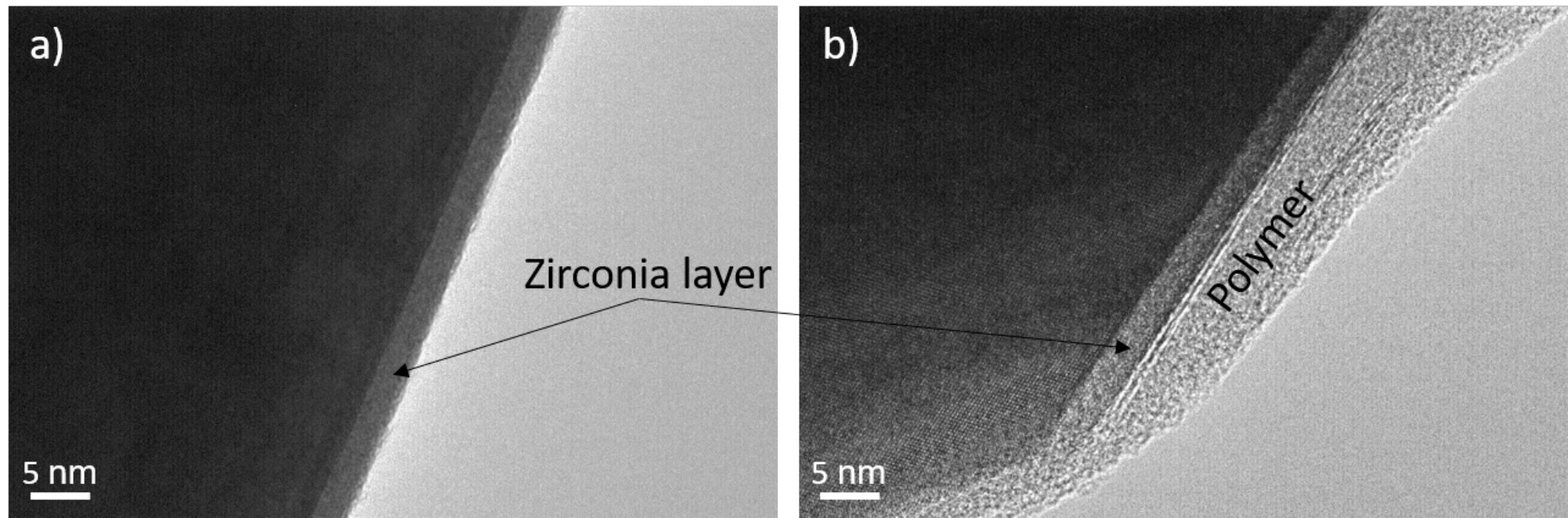
a)
Zirconia layer
5 nm
b)
Polymer
5 nm

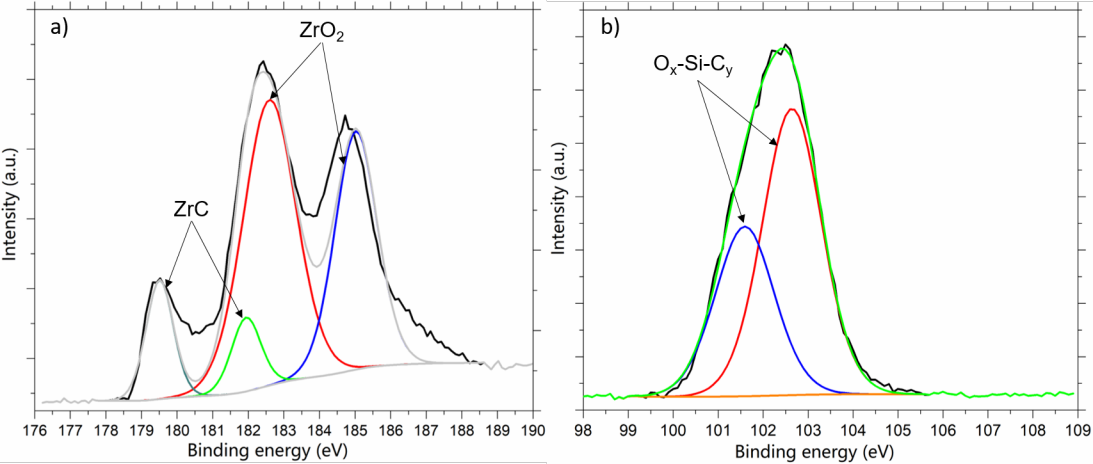
a)
ZrO2
ZrC
Intensity (a.u.)
176 177 178 179 180 181 182 183 184 185 186 187 188 189 190
Binding energy (eV)
b)
Ox-Si-Cy
Intensity (a.u.)
98 99 100 101 102 103 104 105 106 107 108 109
Binding energy (eV)

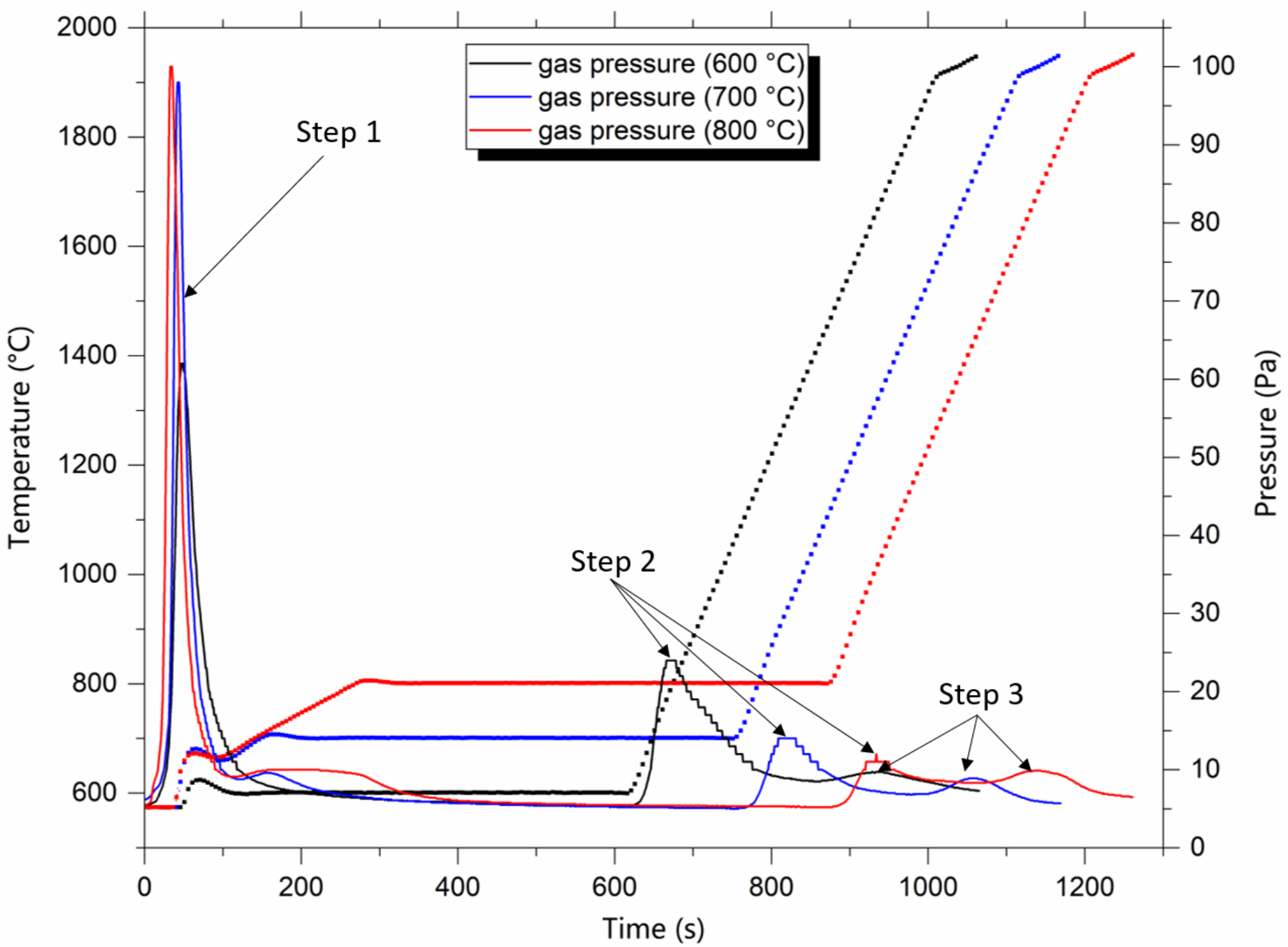
gas pressure (600 °C)
gas pressure (700 °C)
gas pressure (800 °C)
Step 1
Step 2
Step 3
Temperature (°C)
Pressure (Pa)
Time (s)
2000
1800
1600
1400
1200
1000
800
600
100
90
80
70
60
50
40
30
20
10
0
0
200
400
600
800
1000
1200

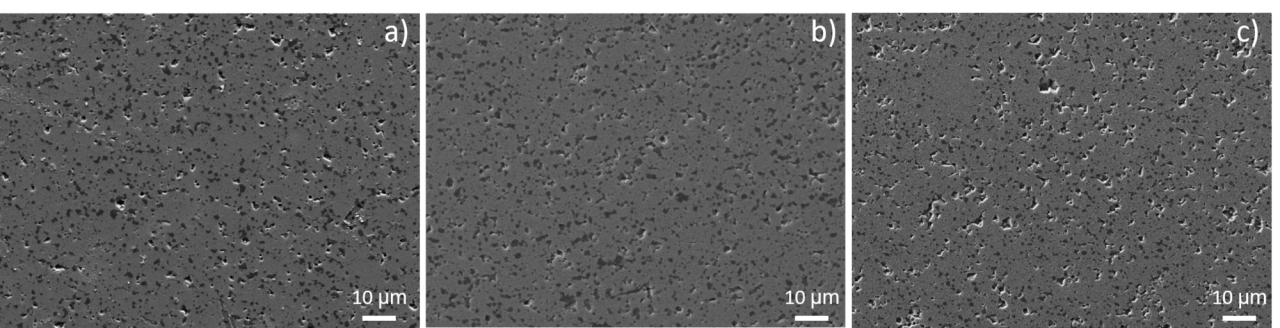
a)
10 µm
b)
10 µm
c)
10 µm

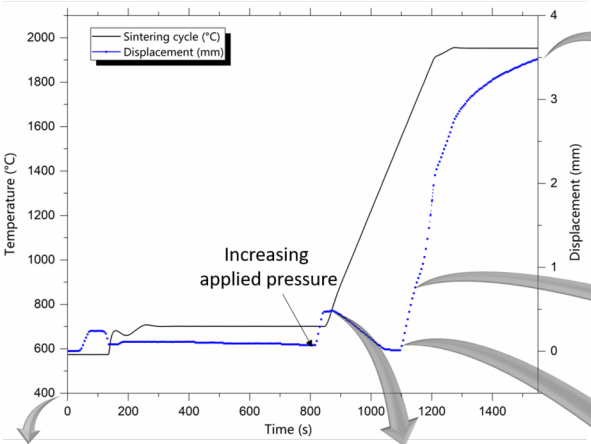

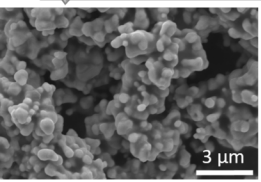

T°= 25 °C
Powder coated with polymer

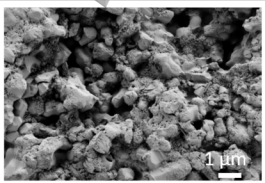

T°= 800 °C
Polymer to ceramic conversion
$P_{open} = 35.7\%$

Step 1 : Rearrangement and bridging between particles

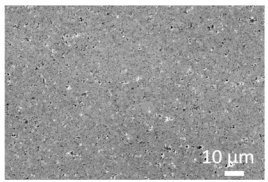

T°= 1550 °C
Start of sintering
$P_{open} = 23.6\%$

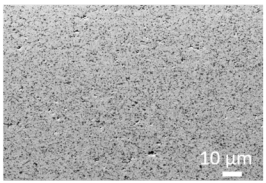

T°= 1700 °C
$P_{open} = 0.7\%$

Step 2 : Elimination of open porosity and densification

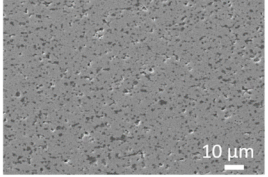

T°= 1950 °C
End of sintering
$P_{open} = 0.9\%$

Step 3 : Coarsening of SiC phase and growth of porosity

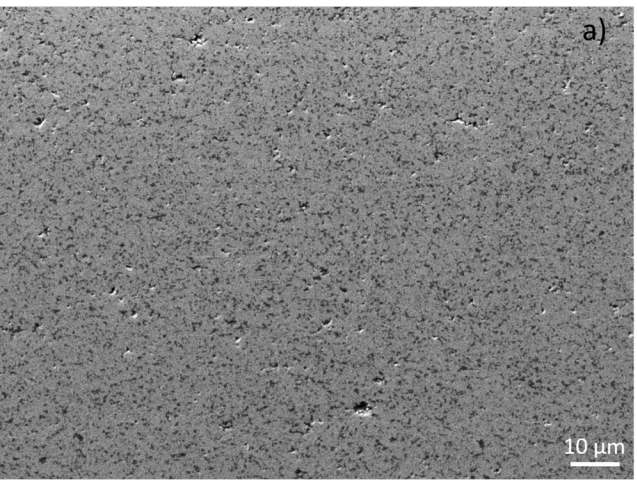
a)
10 µm

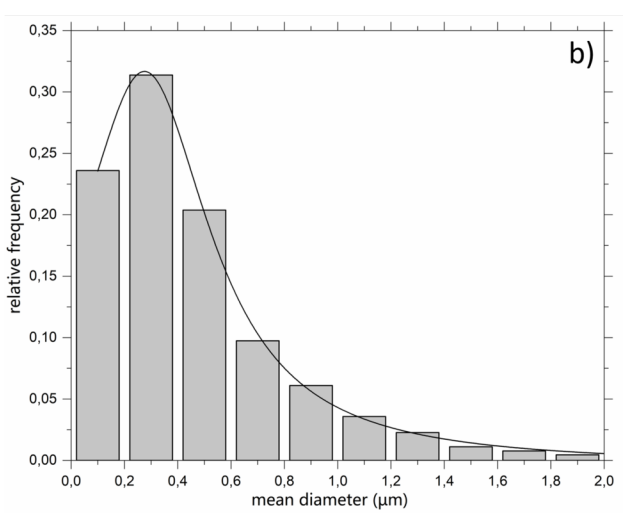
b)
relative frequency
mean diameter (µm)
0,00
0,05
0,10
0,15
0,20
0,25
0,30
0,35
0,0
0,2
0,4
0,6
0,8
1,0
1,2
1,4
1,6
1,8
2,0

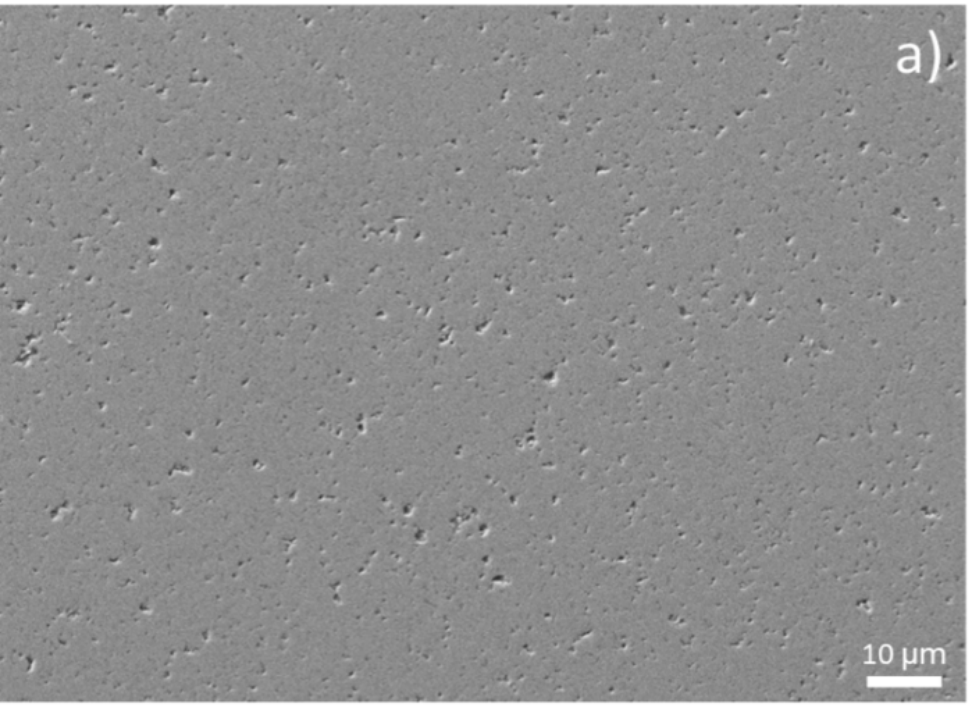
a)
10 µm

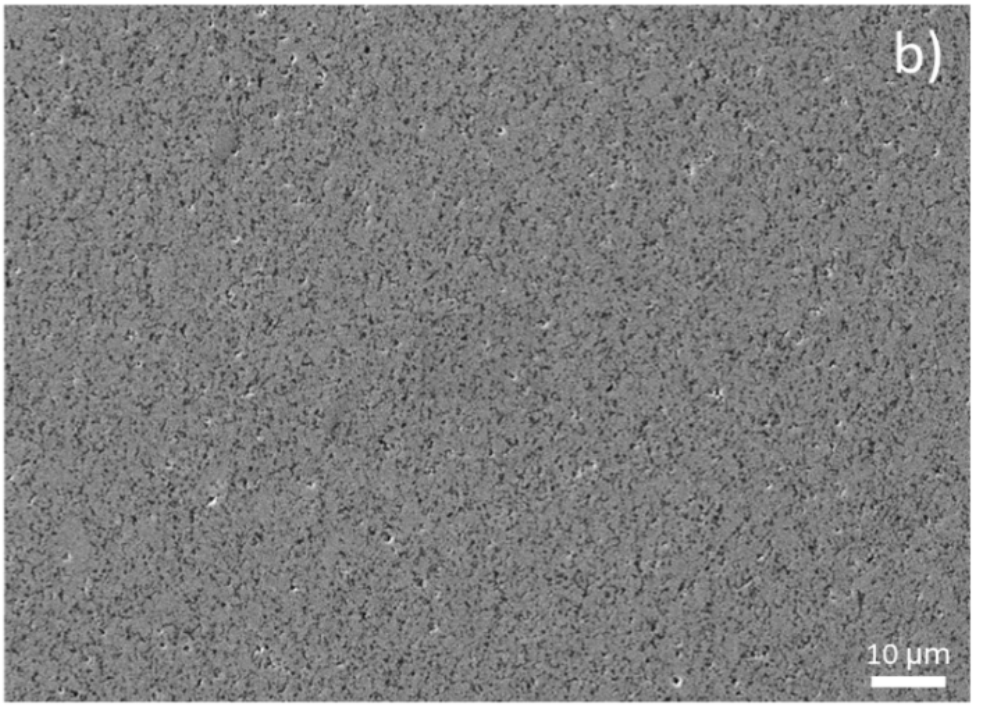
b)
10 µm

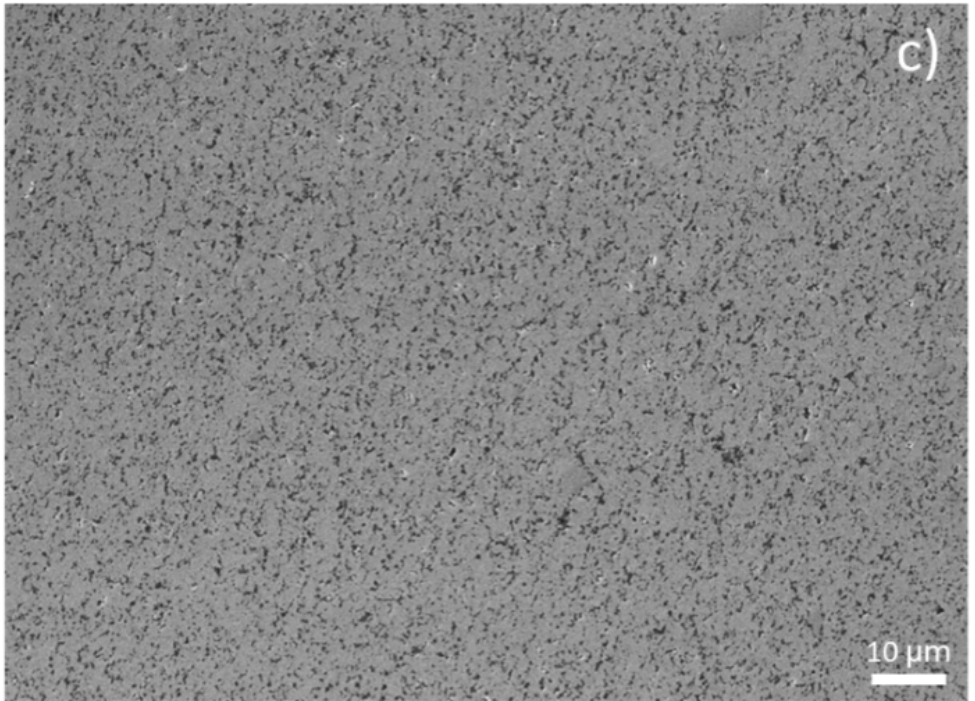
c)
10 µm